Droplet Transport on a Discrete Wettability Gradient Surface: Role of Droplet Weber Number

Visakh Vaikuntanathan*, R. Kannan, D.Sivakumar
Department of Aerospace Engineering,
Indian Institute of Science-Bangalore,
Bangalore – 560 012, India.

Abstract

Understanding droplet motion on wettability gradient surfaces has received considerable academic interest in the context of controlled motion of droplet liquid in a specified direction in micro-scale devices such as biochips. The present work deals with the impact of water droplets of low Weber number (*We*) onto solid surfaces comprising of a discrete gradient of roughness (and hence wettability). Two stainless steel solid surfaces – *TGS1* and *TGS2* – each comprising of a smooth and a parallel groove-textured portion and differing only in the geometry of the textured portion were used. Water droplets of diameter ~ 2.6 mm were impacted onto the interface of the roughness gradient from different heights simulating different *We*. Bulk droplet motion perpendicular to the groove direction was considered. The outcomes of the droplet impact experiments were elucidated in terms of factors significant from the point-of-view of droplet transport: (1) the final horizontal distance moved by the droplet from the impact point, (2) the final contact diameter of the droplet, (3) receding intensity of the droplet fronts on either sides of the interface, and (4) amplitude of droplet oscillations at the final stage of droplet transport. With an increase in impact *We* all the above-mentioned droplet transport parameters deteriorated for both the surfaces indicating a less efficient droplet transport at higher impact Weber numbers. This can be understood qualitatively via energy considerations. Moreover, for a given impact condition, the droplet transport parameters were found to be superior in the case of *TGS2* surface. Attempts were made to explain this behavior in terms of the relative magnitude of wettability gradient (or the difference between the equilibrium contact angles of water on smooth and textured portions) and contact angle hysteresis on these solid surfaces.

1. Introduction

The significance of understanding and controlling the interaction of a liquid droplet with a solid surface can be understood from the host of practical applications like ink-jet printing, self-cleaning surfaces, pesticide deposition onto leaf surfaces, spray coating, spray cooling, microfluidic droplet transport for bio- and chemical-related assays, etc. The motivation also comes from the sheer beauty of natural phenomena like liquid droplets bouncing off lotus leaves [1], desert beetles harvesting water using their body texture [2], the anisotropic nature of leaves of rice plant [3] and butterfly wings [4] which causes directional run-off of liquids, and a myriad of features seen among the flora and fauna of nature.

In order to understand how a liquid droplet, with or without significant inertia, interacts with a solid surface (smooth, randomly rough, or textured with pillars, posts, grooves of various cross sections and sizes), experimental as well as theoretical studies of a liquid droplet spreading on such solid surfaces were conducted by several research groups. A variety of physical events – spreading, receding, splashing, bouncing – associated with the impact of a liquid droplet onto a smooth solid surface were observed experimentally and in numerical simulations [5]. Further, how the above events are modified in the case of a conventional rough surface (with random roughness features and characterized by a R_a or R_q value) were looked into. In order to understand the effect of individual roughness dimensions on the above processes, textured surfaces with well-defined roughness features were used [6]. Also, interesting and practically significant phenomena like entrapment of an air bubble inside the liquid droplet and ejection of a high speed liquid jet from the impacted liquid droplet were observed for particular ranges of impact Weber number and for a given combination of liquid and solid [7, 8]. To study the behavior of liquid droplets impacted onto smooth, conventional rough, and textured rough surfaces, the advancing and receding motions of three-phase contact line have to be understood first. For this, the equilibrium, advancing, and receding contact angles of the liquid droplet on such surfaces have to be determined experimentally.

Various techniques have been employed to control and manipulate the behavior of liquid droplets on solid surfaces, thus enabling to transport them in a preferred manner. The fundamental idea behind these techniques is to create a gradient in surface tension or the curvature of the liquid droplet deposited on a solid surface. The force resulting from this surface tension or curvature gradient drives the liquid droplet. For achieving bulk transport of the liquid droplet over the solid surface, the driving force should be greater than the resistive force due to contact angle

* Corresponding author, visakh@aero.iisc.ernet.in

hysteresis. By creating a thermal gradient on the solid surface, a gradient of surface tension and hence the curvature of liquid droplet could be developed [9, 10]. The Marangoni force developed due to this surface tension gradient (with or without external vibration) aids the droplet motion. Other techniques employed to create a liquid droplet curvature gradient include electro-wetting [11, 12], chemical gradient on the solid surface with or without external vibration [13-17], light-induced droplet motion [18], and physical texture gradient on the solid surface [19-26] (or a combination of these techniques). Of the above techniques, thermal gradient, electro-wetting, magnetic field, and light-induced droplet motion belong to the class of active control of droplet motion as they enable on-site (live) droplet manipulation. The techniques of droplet manipulation by chemical and physical texture gradient on the solid surface are mostly passive. But, a method to dynamically switch the wettability of a physically structured solid surface was reported, thus making it possible to actively control droplet motion [27]. Also, it was pointed out that the techniques other than physical texture gradient may be intrusive, in that the technique employed may alter the properties of the liquid droplet [22]. This may be a serious concern in applications involving bio- and chemical assays.

Most of the work on droplet manipulation/transportation on solid surfaces dealt with the case of a liquid droplet with no impact velocity ($We \sim 0$). Different methods by which liquid droplets can be transported and manipulated on solid surfaces for such cases and the advantages and disadvantages of each of them were reported. But, when practical applications like window-cleaning, spray cooling, liquid deposition, etc. are considered, the impact velocity of liquid droplet is non-zero. Thinking futuristically, when continuous wettability gradient surfaces will be employed in such applications, an understanding of the effect of impact velocity on droplet transport process is essential.

2. Materials and Methods

The experimental set-up employed to perform liquid droplet impact studies on wettability-gradient surfaces consists of the following components: (1) target surfaces, (2) liquid droplet delivery system, and (3) video acquisition system. The details of each of these components are given in the following text.

2.1 Target surfaces

Two solid stainless steel (grade 304) surfaces – *TGS1* and *TGS2* – are used. Both the surfaces consist of a "smooth" portion and a textured portion. The textured portion (denoted by *TS1* and *TS2*) is made of parallel groove-like structures with pillar-like structures separating two adjacent grooves. On a particular surface, the entire textured portion is characterized by such grooves and pillars of constant width and depth. The difference between the two surfaces is in the dimensions of the groove and pillar structures on the textured portion. The smooth portion on both the surfaces exhibits a roughness value (R_a) of ~ 0.013 μm. The geometrical parameters of the textured portions, calculated from video microscope images, are as follows: *TS1*: Groove depth, h = 140 μm; groove width, w_g = 173 μm; pillar width, w_p = 126 μm and *TS2*: Groove depth, h = 220 μm; groove width, w_g = 173 μm; pillar width, w_p = 126 μm. The smooth portions on *TGS1* and *TGS2* will be referred to as *RS1* and the textured portions on *TGS1* and *TGS2* will be referred to as *TS1* and *TS2* respectively.

2.2 Liquid droplet delivery system

The liquid (water) droplet delivery system consists of a micrometer-syringe-needle arrangement. Distilled water stored in the syringe is pushed with the help of micrometer and delivered as droplets through the flat-tipped hypodermic needle (the inner and outer diameters are 0.25 *mm* and 0.37 *mm* respectively). The diameter of the water droplet (D_o) is approximately 2.6 *mm*. The properties of liquid water used are: dynamic viscosity, $\mu = 0.89 \times 10^{-3}$ *kg/(m.s)*; surface tension, σ = 0.073 *N/m*; and density, ρ = 996 kg/m^3 [28]. The water droplets are impacted onto the target surfaces from different heights simulating different impact Weber number (*We*) conditions.

2.3 Video acquisition system

The video acquisition system consists of a high speed video camera, a LED light source, and a software for controlling the high speed camera operation and visualizing the captured frames. In the present experimental study, images of the droplet impact process are captured at a rate of 5000 frames per second and a total of 1000 frames were used for further measurements (the entire set of events in droplet impact occurs within this time interval).

The water droplet is impacted onto the interface of smooth and textured portions of the surfaces. The offset of the initial contact point of water droplet with the solid surface from the interface for each impact condition was minimal. From the captured images, the base contact diameter and location of the three-phase contact points on either sides of the interface are measured. The temporal variations of the distance of three-phase contact points from the interface/initial contact point, distance of the midpoint of droplet baseline from the initial contact point, and base contact diameter are plotted for a range of *We* for the two surfaces. From these plots, quantities relevant from a droplet transport perspective are measured. The details of measurement of these quantities and the effects of impact *We* and surface wettability on them are presented in the following sections.

The equilibrium contact angles and contact angle hysteresis of water on smooth (*RS1*), structured portion of *TGS1* (*TS1*), and structured portion of *TGS2* (*TS2*) were also experimentally measured. For determining contact angle hysteresis, the advancing contact angle was measured by captive-needle volume addition process and the receding contact angle by droplet evaporation under ambient condition. The relevant wettability data for the surfaces studied here are as follows: *RS1*: Equilibrium contact angle, $\theta_{eqm} = 76^0$; advancing contact angle, $\theta_{adv} = 76^0$; *TS1*: Equilibrium contact angle (perpendicular to the grooves), $\theta_{eqm} = 126^0$; receding contact angle (perpendicular to the grooves), $\theta_{rec} = 100^0$; *TS2*: Equilibrium contact angle (perpendicular to the grooves), $\theta_{eqm} = 135^0$; receding contact angle (perpendicular to the grooves), $\theta_{rec} = 120^0$.

3. Results and Discussion

The processes occurring during the spreading of a liquid droplet on the wettability-gradient surfaces and their final outcome are quantified here in terms of the following – (1) the final distance moved by the midpoint of droplet baseline from the initial contact point, (2) the final base contact diameter of the liquid droplet, and (3) the time evolution of the distance of three-phase contact points on either sides of the interface. The influence of the following parameters on the above processes and their outcomes are considered – (i) the impact kinetic energy (or the Weber number) and (ii) the surface structure (or the wettability).

3.1 Final distance moved by the midpoint of droplet baseline from the initial contact point

Fig. 1(a) shows the effect of impact Weber number and surface structure on the final distance moved by the midpoint of droplet baseline from the initial contact point. It can be seen that for both the surfaces the final distance moved decreases with increase in impact Weber number. This can be explained as follows: As the impact Weber number increases, the kinetic energy with which the liquid droplet impacts on the solid surface increases. This equips the liquid droplet front spreading towards the structured portion of solid surface with more energy (when compared to a lower *We*) to overcome the energy barriers posed by the pillar edges. As a result of this, the droplet front advances more in the direction of textured portion when compared to a lower Weber number case. This is clearly seen in Fig. 1(b). Hence the amount of energy dissipated will be more and that aiding the bulk droplet transport along the wettability gradient will be less in the case of a higher Weber number. Also, the maximum spreading on the smooth portion is greater than that on the structured/textured portion for all Weber numbers. The obvious reason for this is the absence of resistance due to energy barriers on the smooth portion. However, the maximum spreading on the smooth portion is seen to be almost independent of the impact Weber number.

Another observation from Fig. 1(a) is the effect of surface structure on droplet transport. It can be clearly seen that, for all Weber numbers, *TGS2* offers a better droplet transport than *TGS1*. This can be explained by considering the equilibrium contact angle and contact angle hysteresis of a water droplet on these surfaces. The force aiding the droplet transport across the interface is proportional to the wettability gradient (decided by the equilibrium contact angles of a water droplet on the smooth and textured portions) and the force resisting the droplet transport is proportional to the contact angle hysteresis of a water droplet on the smooth and textured portions of the surface. When a liquid droplet moves from the textured portion to the smooth portion, it "recedes" from the textured portion and "advances" on the smooth portion. Hence the contact angles corresponding to these events are the relevant ones – advancing contact angle on *RS1* and receding contact angles on *TS1* and *TS2*. Since the equilibrium and advancing contact angles on *RS1* is common for both the surfaces *TGS1* and *TGS2*, the textured portion with higher equilibrium and receding contact angles (*TGS1*) is expected to show better droplet transport properties.

3.2 Final base contact diameter of the liquid droplet

The final distance moved by the midpoint of baseline of liquid droplet, as studied in the above section, gives an estimate of only the distance to which the midpoint (or roughly speaking, the center of mass) of the liquid droplet is transported. A particular position of the midpoint of baseline can correspond to different positions of the contact points and hence different final contact diameters. As far as droplet-based microfluidic systems – in which small volumes of liquid are transported from a source to sink (for applications like chemical analysis and bioassay) – are concerned, the final droplet shape should be as compact as possible with minimal spreading so that the intended volume of liquid can be *completely* delivered to the destination/sink. Keeping this requirement in mind, the effects of impact Weber number and surface wettability on final contact diameter of the liquid droplet are studied in the following text.

The final base contact diameters of the liquid droplet for different impact Weber number conditions for the two surfaces were measured from contact diameter versus time plots. Fig. 2 helps in comparing the final contact diameters on the two surfaces for all impact conditions. It can be seen that for all impact conditions the points fall below the 45 degree line which implies that the final contact diameter on *TGS2* surface is less than that on *TGS1* for all

impact cases studied. But since most of the points lie very close to the 45 degree line, it may be concluded that on both the surfaces the final contact diameter is similar (taking into account experimental errors).

If the final position of the water droplet is (almost) entirely on the smooth portion then, irrespective of *TGS1* or *TGS2*, the final contact diameter will be the same for a particular *We*. Hence the behavior as seen in Fig. 5 is expected.

3.3 Time evolution of the three-phase contact points on either sides of the interface

The above two sections dealt with the effect of impact Weber number and surface wettability on the final distance to which the droplet is transported and the final spreading of the liquid droplet. These studies are significant from an application point of view. However, it is also important to understand how various events taking place during the entire droplet spreading process affect these outcomes. Let us now consider a typical plot showing the temporal variation of the distance of three-phase contact points on either sides of the interface from the initial contact point (Fig. 3(a)). Such a plot may be divided into three distinct time periods:

Period I: This corresponds to the initial kinematic stage in the spreading of droplet in which the kinetic energy of the droplet plays a dominant role overshadowing the effects due to surface structure. Hence the liquid fronts on either sides of the interface show similar trend with time. Both the liquid fronts spread to a maximum during this period. But it can be noticed that the maximum spreading of the liquid front on the smooth portion is greater than that on the textured portion. The liquid front advancing on the textured portion encounters energy barriers in the form of pillar edges. A portion of the droplet's kinetic energy will be consumed to overcome these energy barriers. Since the smooth surface offers no such resistance to the droplet front's motion, the primary spreading maximum along the smooth surface may be expected to be more than that along the textured portion.

Period II: During this time period the droplet fronts start receding. The amount of receding (quantified by decrease in the distance of droplet front/three-phase contact point from the initial contact point) is more on the textured portion. The intense receding along the textured portion forces the droplet front on the smooth portion to advance. This characteristic motion of the droplet fronts – intense receding along the textured portion and advancing along the smooth portion – results in bulk transport of the droplet across the surface. The receding intensity during the first receding process on the textured portion is much greater than that on the smooth portion. Also, multiple receding on the smooth portion and multiple advancing on the textured portion are undesirable from the point of view of droplet transport. Since the initial processes play a decisive role in droplet transport along the wettability gradient, it is further looked into in the following text. The intensity of primary receding process (expressed in *mm/s*) along smooth and textured portions is calculated as the slope of the (almost) straight line representing the receding process in Fig. 3(a). Fig. 3(b) shows the variation of primary receding intensity on *TS1*, *TS2*, and their corresponding smooth portions. It may be noted that receding intensity on all surfaces increase with increase in impact Weber number. As the impact Weber number increases, the liquid droplet will be equipped with more kinetic energy which can be utilized in the receding process [Here, it should be noted that although the receding intensity increases with Weber number, the final distance moved by the midpoint of droplet baseline is seen to decrease with Weber number (Fig. 1(a)). This is because as the Weber number increases the maximum initial spreading along the textured portion also increases (Fig. 1(b))]. Further, the receding intensity is seen to be more on *TS2* than on *TS1* for all impact conditions studied (which shows the effect of surface wettability). This makes *TS2* a better candidate for droplet transport when compared to *TS1*. The receding process on the smooth portion of both these surfaces is seen to follow the same trend with impact Weber number. And, the receding intensity on smooth portion is less than that on the corresponding textured portion for all impact cases studied here.

The above observations may be explained as follows: The liquid droplet (for non-impact equilibrium case) occupies the Cassie-Baxter configuration on the textured portions of both *TS2* and *TS1* surfaces. The ambient air trapped inside the channels offers a cushion-like support, makes the surface hydrophobic on an average, and reduces the resistance to droplet's receding motion when compared to the smooth surface. Also, since the channel depth of *TS2* surface is more than that of *TS1* surface, there is chance of more air getting entrapped inside the channels and hence lesser resistance. From these, it may be concluded that the receding intensity on *TS1* is more than that on smooth portion but less than that on *TS2*.

Period III: This corresponds to the events after the bulk receding and advancing processes. Once both the contact points are located on the smooth portion of the surface they oscillate about this final equilibrium position – the amplitude of oscillation being higher for a higher impact Weber number. This stage doesn't hold much significance to the phenomenon of bulk droplet transport. However, for practical applications a minimum amplitude of these oscillations is generally desirable as oscillations with less amplitude and hence having less energy (energy of an oscillation is proportional to the square of its amplitude) can be damped more easily and the liquid droplet will attain its final equilibrium shape faster.

Conclusions

The present work was aimed at studying the effects of impact Weber number and surface wettability on bulk liquid droplet transport across discrete wettability gradient surfaces comprising a smooth and a textured portion. The main conclusions of the work can be summarized as follows:

- On a given wettability gradient surface, an increase in droplet impact Weber number deteriorates the droplet transport process. This was qualitatively explained with the concept of energy barriers. Future work should also focus on high *We* regimes.
- For a given droplet impact Weber number, the surface with a higher wettability gradient and higher receding contact angle on textured portion shows better droplet transport properties. Although the surfaces studied here showed a difference in droplet transport properties, a future study should include surfaces with a wider range of wettability gradients and contact angle hysteresis to arrive at a stronger conclusion.
- Further, the individual events involved in droplet transport process were studied using a typical temporal plot of droplet front position. Dividing the entire plot into three distinct regions, it was shown that the receding intensities on the textured portions is one of the important factors governing the droplet transport process.

Acknowledgements

The authors would like to thank Prof. G. Jagadeesh and Mr. R. Sriram of High Enthalpy Aerodynamics Lab, Department of Aerospace Engineering, Indian Institute of Science Bangalore for providing access to and helping with the high speed camera facility.

References

[1] A. Otten, S. Herminghaus, Langmuir (2004) 20 2405-2408.
[2] C. Dorrer, J. Ruhe, Langmuir (2008) 24 6154-6158.
[3] Z. Guo, W. Liu, Plant Science (2007) 172 1103-1112.
[4] Y. Zheng, X. Gao, L. Jiang, Soft Matter (2007) 3 178-182.
[5] A. L. Yarin, Ann. Rev. Fluid Mech. (2006) 38 159-92.
[6] D. Quere, Physica A 313 (2002) 32-46.
[7] D. Bartolo, C. Josserand, D. Bonn, PRL (2006) 96 124501.
[8] S. T. Thoroddsen, T. G. Etoh, K. Takehara, N. Ootsuka, Y. Hatsuki, J. Fluid Mech. (2005) 545 203-212.
[9] A. A. Darhuber, J. P. Valentino, S. M. Troian, S. Wagner, Journal of Microelectromechanical Systems (2003) 12 873-879.
[10] S. Mettu, M. K. Chaudhury, Langmuir (2008) 24 10833-10837.
[11] S. K. Cho, H. Moon, C. –J. Kim, Journal of Microelectromechanical Systems (2003) 12 70-80.
[12] L. Latorre, J. Kim, J. Lee, P-P de Guzman, H. J. Lee, P. Nouet, C. –J. Kim, Journal of Microelectromechanical Systems (2002) 11 302-308.
[13] S. –W. Lee, D. Y. Kwok, P. E. Laibinis, Phys. Rev. E (2002) 65 051602.
[14] R. J. Petrie, T. Bailey, C. B. Gorman, J. Genzer, Langmuir (2004) 20 9893-9896.
[15] S. –H. Choi, B. Z. Newby, Langmuir (2003) 19 7427-7435.
[16] S. Daniel, S. Sircar, J. Gliem, M. K. Chaudhury, Langmuir (2004) 20 4085-4092.
[17] S. Daniel, M. K. Chaudhury, Langmuir (2002) 18 3404-3407.
[18] K. Ichimura, S-K. Oh, M. Nakagawa, Science (2000) 288 1624-1626.
[19] Jing-Tang Yang, Zong-Han Yang, Chien-Yang Chen, Da-Jeng Yao, Langmuir (2008) 24 9889-9897.
[20] C. Sun, X-W. Zhao, Y-H. Han, Z-Z. Gu, Thin Solid Films (2008) 516 4059-4063.
[21] A. Shastry, M. J. Case, K. F. Bohringer, Langmuir (2006) 22 6161-6167.
[22] J-T. Yang, J. C. Chen, K-J. Huang, J. A. Yeh, Journal of Microelectromechanical Systems (2006) 15 697-707.
[23] G. Fang, W. Li, X. Wang, G. Qiao, Langmuir (2008) 24 11651-11660.
[24] L. Zhu, Y. Feng, X. Ye, Z. Zhou, Sensors and Actuators A (2006) 130-131 595-600.
[25] Y. Xiu, L. Zhu, D. W. Hess, C. P. Wong, Nano Letters (2007) 7 3388-3393.
[26] J. Zhang, L. Xue, Y. Han, Langmuir (2005) 21 5-8.
[27] B. He, J. Lee, IEEE The Sixteenth Annual International Conference on Micro Electro Mechanical Systems, 2003. MEMS-03 Kyoto, pp. 120-123.
[28] Pijush K. Kundu, Ira M. Cohen, Fluid Mechanics Third edition, ISBN: 978-81-8147-648-7, pp 735.

List of Figures

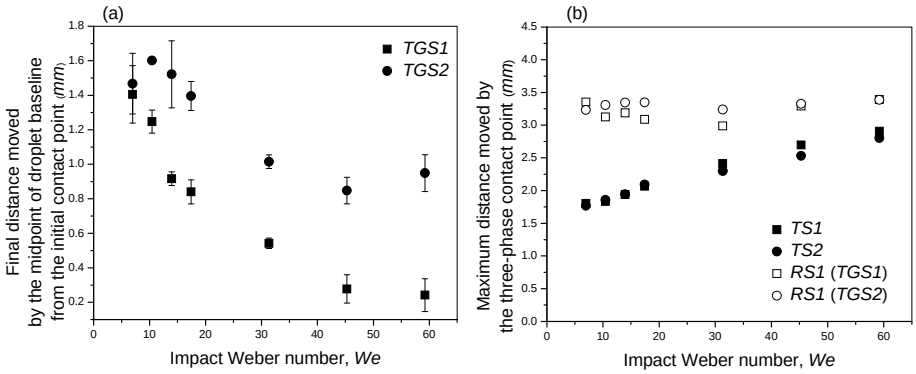

Figure 1. Plots showing the effect of impact Weber number on (a) the final distance moved by the midpoint of liquid droplet baseline and (b) the maximum distance moved by the three-phase contact points (droplet front) from the impact point on the wettability gradient surfaces.

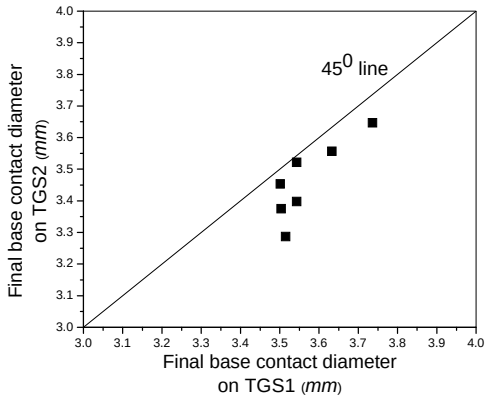

Figure 2. Plot showing a comparison of the final contact diameters on *TGS1* and *TGS2*.

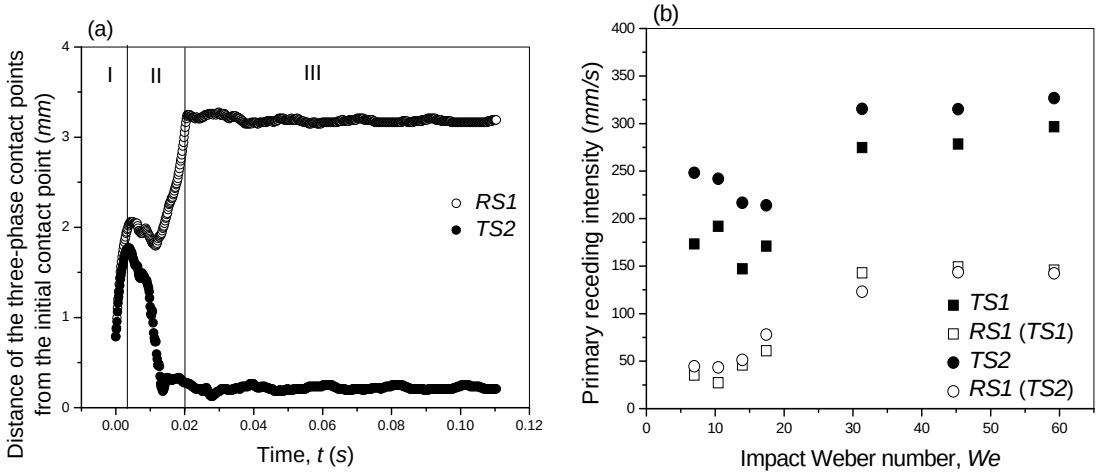

Figure 3. (a) A typical plot showing the time evolution of the three-phase contact points on either sides of the interface. (b) Plot representing the variation of primary receding intensity with the impact Weber number.